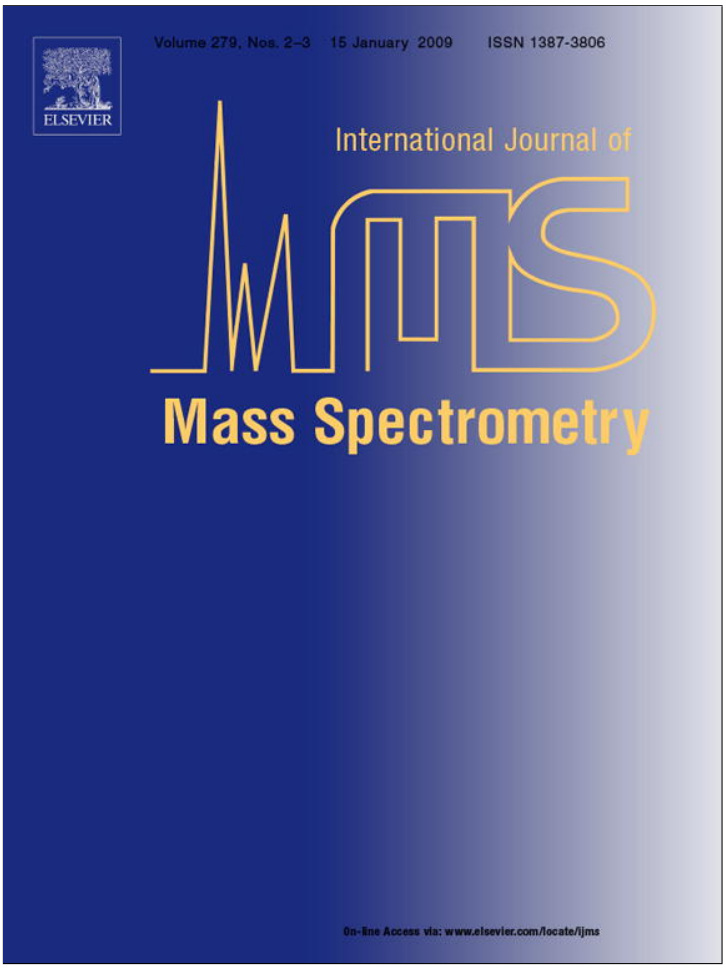

International Journal of Mass Spectrometry 279 (2009) 147–155

Contents lists available at ScienceDirect

International Journal of Mass Spectrometry

journal homepage: www.elsevier.com/locate/ijms

Numerical simulations of kinetic ion temperature in a cryogenic linear multipole trap

Oskar Asvany*, Stephan Schlemmer

I. Physikalisches Institut, Universität zu Köln, Zülpicher Str. 77, 50937 Köln, Germany

ARTICLE INFO

Article history:
Received 16 September 2008
Received in revised form 27 October 2008
Accepted 28 October 2008
Available online 6 November 2008

Keywords:
Multipole ion trap
22-Pole trap
Numerical simulation
Ion temperature
Buffer gas cooling

ABSTRACT

This work presents numerical simulations of the kinetic temperature of ions stored in a linear multipole RF trap (22-pole trap) under the influence of elastic collisions with buffer gas. Small distortions, as for example those caused by the trapping endelectrodes, space charges, or noise on the RF signal, can be included into the model. The dependence of the resultant ion temperature on all storage parameters is systematically investigated. In particular, it is found that an unfavourable ion-to-neutral mass ratio and high trapping endelectrode voltages can lead to ion heating far above the trap temperature.

1. Introduction

Many experiments in the field of atomic and molecular physics prefer to cool the investigated species to cryogenic temperatures, giving the spectroscopic advantage of reduced Doppler line width and sparse population of internal states. There are a variety of methods to achieve this objective, as for example the well-known supersonic expansion, laser cooling of trapped atoms [1], ions [2], or sympathetic cooling of ionic molecules [3]. The most straightforward and generally applicable method used for trapped ions is buffer gas cooling, in which the ions are subject to a (pulsed) buffer gas bath, usually helium, and thereby relax to the temperature of the environment within a few collisions. With buffer gas cooling, minimum temperatures in the range of 4 K can be reached using a suitable cold head or liquid helium.

Applying buffer gas cooling, cases have been reported in which the spectroscopically determined kinetic temperature of the stored ions exceeded the nominal trap temperature [4–6]. While these differences are not problematic for spectroscopy, they pose a severe distortion when studying low-temperature (deuteration) ion-molecule chemistry [7–9]. Possible reasons for the seen discrepancies could be attributed to heating by kinetic energy release in exothermic reactions, heating effects caused by the RF field of a perfect or real (i.e., imperfect) multipole trap, noise on some electrodes, or simply by mechanical parts of the trap with a temperature higher than the nominal (measured) one. In order to separate and quantify the ion heating contributions of a perfect or imperfect trap, simulations of ion motion in a cryogenic multipole trap and the resulting ion temperature have been performed and the results are presented in this work.

Since its advent, the Paul trap [10–12] has been a workhorse for the investigation of all kinds of charged particles. For this reason, there has been early numerical work [13] in order to understand the detailed mass-spectrometric properties of that device, and later these simulations have been extended to include gas collisions and space charge, see for example [14,15] and references therein. Similarly, the behaviour of laser cooled ions in linear Paul traps is well understood [16]. However, there is only little numerical work specialized on linear multipole traps. These traps have a field-free region much wider than conventional Paul traps and are thus well-suited for general low-temperature applications. Gerlich [17] presented energy distributions of ions trapped in different linear multipole traps and a ring-electrode trap in collision with 300 K and 80 K hydrogen gas, and demonstrated the detrimental effects of potential distortions on the energy distribution. More recently, molecular dynamics simulations have been performed to determine the different structures of laser-cooled Ca^+ crystals in a linear octopole trap [18].

This work is dedicated to simulations of buffer gas cooled ions stored in linear multipole traps. Special attention is paid to Gerlich's 22-pole trap [19], as this kind of trap became a standard tool for the spectroscopic and reactive characterization of cold ions

* Corresponding author.
E-mail address: asvany@ph1.uni-koeln.de (O. Asvany).

1387-3806/$ – see front matter © 2008 Elsevier B.V. All rights reserved.
doi:10.1016/j.ijms.2008.10.022

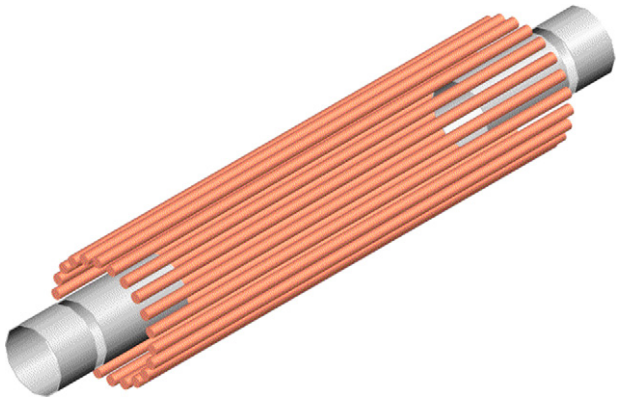

Fig. 1. Sketch of the 22-pole ion trap. Ion confinement in radial direction is achieved by applying a RF voltage to the 22 small rods, while longitudinal confinement is controlled by the inner cylindrical endelectrodes.

[4–6,9,20–26]. After a presentation of its geometry and the chosen operating parameters in Section 2, the applied computational methods are outlined in Section 3 and test runs of the code are presented (Section 4). Thereafter, ion velocity distributions and the deduced ion temperatures are presented for an infinitely long 22-pole trap (Section 5) under varying parameters. The effect of the endelectrodes (Section 6) used for longitudinal confinement and trap imperfections (Section 7) are also discussed. Finally, a conclusion is drawn about the temperature differences seen in our laboratory [5,6] and an outlook is given for the applicability of the presented methods for the design of future multipole traps with in situ mass-selection capabilities.

2. Trap geometry and operating parameters

The trap geometry considered here is a 22-pole ion trap [19] as shown in Fig. 1. It consists of 22 small rods (each 1 mm diameter, 3.7 cm long) which circumscribe a cylinder of $r_0 = 5$ mm radius. The two phases of an RF voltage with amplitude V_0 and frequency f are applied to the 2×11 rods, confining the ions in the radial direction. For the confinement in longitudinal direction, two 6.6 mm inner diameter cylindrical electrodes (the inner ones shown in Fig. 1), called endelectrodes, are held at a positive voltage V with respect to the trap potential. The trap is usually mounted on a closed-cycle helium refrigerator, which cools the admitted gases to the temperature T. The remainder of this paper is concerned with how the buffer gas temperature is transmitted to the ion kinetic temperature, depending on the parameters introduced above. Oriented at our earlier experiments [5], the standard conditions summarized in Table 1 were chosen for the simulations.

3. Computational methods

For the numerical simulations, the program Labview 7.1 under a Linux operating system has been chosen as it offers easy handling, visuality, and predefined routines. Newton's equations of motion are integrated for one singly charged ion of mass m in three dimensions. Doing small time steps of fixed length (1/50 of the RF period has proven to be sufficient in most cases), the change of the ion position and velocity is calculated and added. The so-called leapfrog algorithm was used [27]. Higher Runge–Kutta integration methods have not been applied to keep the program simple, and because high precision was not necessary as usually buffer gas collisions randomize the ion velocity. Following the motion of the single ion in the trap, distributions of its position and/or velocity can be sampled in regular or random time intervals. As we were primarily interested in the ion kinetic temperature, mostly distributions of the velocity magnitude $v = \|\vec{v}\|$ were recorded. This velocity distribution corresponds to the one obtained for an ensemble of many ions at one instant. The temperature of the ion ensemble can then be defined by

$$T = \frac{\pi m \bar{v}^2}{8k} \tag{1}$$

where $\bar{v}$ is the mean of the (in general non-Maxwellian) velocity distribution. A sketch of the basic program flowchart is shown in Fig. 2, and in the following the modular ingredients of the program, i.e., the RF field, the buffer gas collisions, the field of the endelectrodes, and the space charge field, are described in more detail.

3.1. Linear multipole RF field

The calculation of the RF-field is straightforward as the analytical expression of the time-dependent potential inside an infinitely long multipole can be used (see e.g., Gerlich [17])

$$\Phi(r, \phi, t) = V_0 (r/r_0)^n \cos(n\phi) \sin(\omega t) \tag{2}$$

where V_0 is the voltage amplitude applied to the $2n$ hyperbolic electrodes enclosing an inner radius r_0, and $\omega = 2\pi f$ is the angular frequency. The electric potentials for different multipolarities n are visualized in Fig. 3 together with some typical ion trajectories. From expression (2) the E-field can be easily derived:

$$\begin{pmatrix} E_x \\ E_y \end{pmatrix} = nV_0 \frac{r^{n-1}}{r_0^n} \begin{pmatrix} -\cos((n-1)\phi) \\ \sin((n-1)\phi) \end{pmatrix} \sin(\omega t). \tag{3}$$

Note that the E-field above is given in Cartesian coordinates, while its dependency is in polar coordinates r and ϕ. Although the above E-field is exactly valid only for a pure multipole field (i.e., for electrodes with perfect hyperbolic shape), the above formula with $n = 11$ is a very good approximation for a 22-pole trap (shown in Fig 1), as calculations reveal that the contribution of higher order multipoles ($n = 33, 55, 77, \ldots$) due to the circular electrode shape (instead of hyperbolic ones) is less than 2%.

3.2. Calculation of electrostatic fields

If desired, electrostatic fields can be included into the simulations, for example those generated by the cylindrical endelectrodes (see Fig. 1) in order to confine the ions in longitudinal direction. Electrostatic fields are calculated by a separate Labview routine which uses the relaxation method similar to that applied by Simion [28]. Simion itself has not been used as its capabilities to export data (as for example potential data files) are limited. The numerical solution of the Laplace equation, $\Delta\Phi(x, y, z) = 0$, works as follows

Table 1
Chosen parameters for numerical simulations.

Inner radius	Ion mass	RF			Buffer gas		
		Multipolarity	Frequency	Amplitude	Mass	Temperature	Collision rate
$r_0 = 5$ mm	$m = 4$ u	$n = 11$	$f = 17$ MHz	$V_0 = 15$ V	$m_b = 4$ u	$T = 18$ K	$R \approx 10^5$ s^{-1}

The ion and buffer gas masses of H_2D^+ and He were considered [5,6]. The buffer gas collision rate corresponds to a He density of about 10^{-14} cm^{-3}.

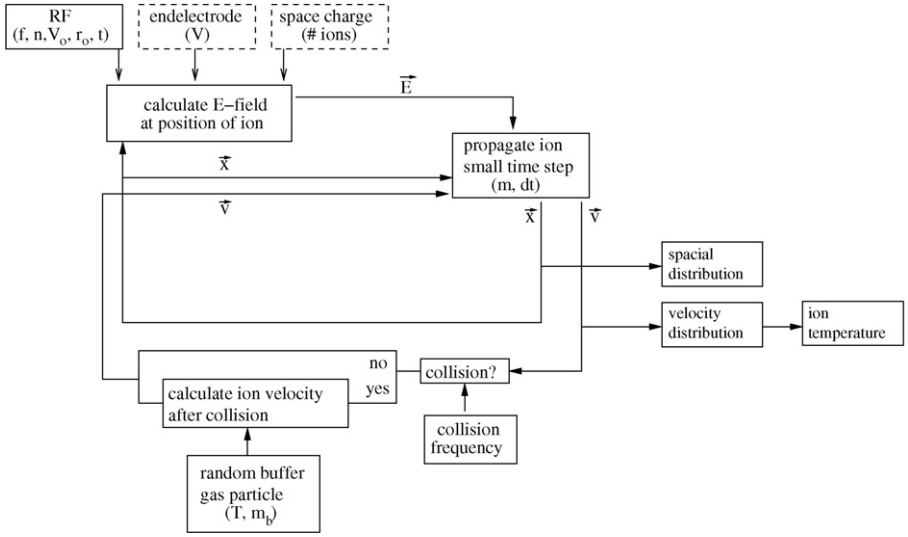

Fig. 2. Flowchart of the simulations. After choosing some initial conditions for the position $\vec{x}$ and velocity $\vec{v}$ of one ion with mass m, it is propagated in the clockwise loop by small time steps Δt: $\Delta\vec{v} = \vec{E}e/m\Delta t$ and $\Delta\vec{x} = \vec{v}\Delta t$. The $\vec{E}$-field at the current ion position is the time-dependent RF-field (Eq. (3)), and if required, additional modules for the electrostatic field of the endelectrodes or the space charge can be added. Once in a while, the velocity of the ion is changed by an elastic collision with a buffer gas particle of mass m_b. The parameters involved in each calculation step are shown in brackets. By executing the shown calculation loop repeatedly, distributions of, e.g., the ion velocity can be obtained, from which the ion temperature is derived by Eq. (1).

[29]: respecting the symmetry of the problem, the space is divided into equidistant cells and those cells coinciding with electrodes are assigned the applied voltage. The potential distribution of the space between the electrodes can then be obtained in an iterative procedure, in which each cell is assigned the mean potential of its neighbouring cells (with appropriate weighting factors for non-Cartesian symmetries). As this iterative method can be quite slow for a two-dimensional problem with, e.g., 1000×1000 cells, it can be speeded up by initially boosting the potential changes of each cell by a certain factor $f \leq 1.9$, and/or by starting with a rough cell division, and gradually decreasing the cell sizes to the desired finesse [28].

Due to the wide field-free region of a 22-pole trap, the RF field cancels out at the position of the endelectrodes, see Figs. 1 and 3 ($n = 11$), and therefore the RF field and the electrostatic field of the endelectrodes can be treated separately and later superimposed. For the calculation of the electrostatic field of the endelectrodes, the cylindrical assembly of the 22 rods of the trap has been approximated by a conducting cylindrical shell with radius r_0 (the radius circumscribed by the 22 rods) which is set to zero voltage. This geometrical simplification, only feasible for higher order multipoles, allows us to do the numerical solution of the Laplace equation with azimuthal symmetry and obtain the field in the form $\Phi(r, z)$. Thus, the calculation is performed for an electrode voltage of 1 V and saved in a two-dimensional data-file $\Phi(r, z)$. This data file can then be read by the ion simulation program, rescaled if necessary for other electrode voltages, and the static E-field obtained by simple numerical derivation.

3.3. Buffer gas collisions

For the collisions of the stored ion with polarizable buffer gas particles the Langevin theory is used (see Appendix A). The Langevin cross section is given by $\sigma = q/v\sqrt{\pi\alpha/\epsilon_0\mu}$, therefore the rate coefficient $k_L = \sigma v$ is independent of ion velocity, making the computations very simple. Collisions of the simulated ion with buffer gas atoms can thus occur at random times, but with a fixed mean collision frequency. A relatively high collision frequency of $10^5\ s^{-1}$, corresponding to a buffer gas density of about $10^{-14}\ cm^{-3}$, has been chosen in most of the simulations (see Table 1) in order to save computing time, but also some runs at higher and lower collision frequencies have been performed when necessary.

Once a collision has been indicated by a random number generator, a buffer gas particle with given mass m_b and a random velocity obeying a Maxwell–Boltzmann distribution with temperature T is generated. The collision with the ion is then resolved in the center-of-mass (CM) system, and the standard procedure (see for example [14]) for an elastic and isotropic collision is followed: (i) transformation into the mutual CM-system, (ii) giving the ion a random direction in the CM-system after the collision while keeping its velocity magnitude, and (iii) transformation back to the laboratory system. In this simple collision model, the internal degrees of freedom of the collision partners are not taken into account. The proper operation of this procedure has been checked by thermalizing the ions in a buffer gas without the presence of any fields (see Section 4.2).

3.4. Space charge effects

Usually space charge effects can be neglected if only a few thousand ions are stored in a 22-pole trap. This condition holds for most of current 22-pole trap experiments. However, the Coulomb interaction between the stored ions becomes important, and thus has to be incorporated into numerical simulations, in cases of either heavy loading of the ion trap (for example when the ion trap is used as a source for a storage ring [21]), or when sufficiently low temperatures enable the formation of a Coulomb crystal [16,18]. In the latter case, the time-consuming explicit computation of the mutual Coulomb interactions is mandatory. For the purposes of a 22-pole trap, however, the simple geometry and the mean-field approximation can be used to estimate the ion temperature.

Assuming an infinitely long 22-pole trap, first the cylindrically symmetric charge distribution established under the influence of its own space charge and the trap potential has to be determined. This can be found in an iterative way, by starting with a charge distribution $\rho_0(r)$, calculating its electric potential $\Phi_0(r)$ by numerical integration of the Poisson equation $\Delta\Phi = -\rho/\epsilon_0$ in

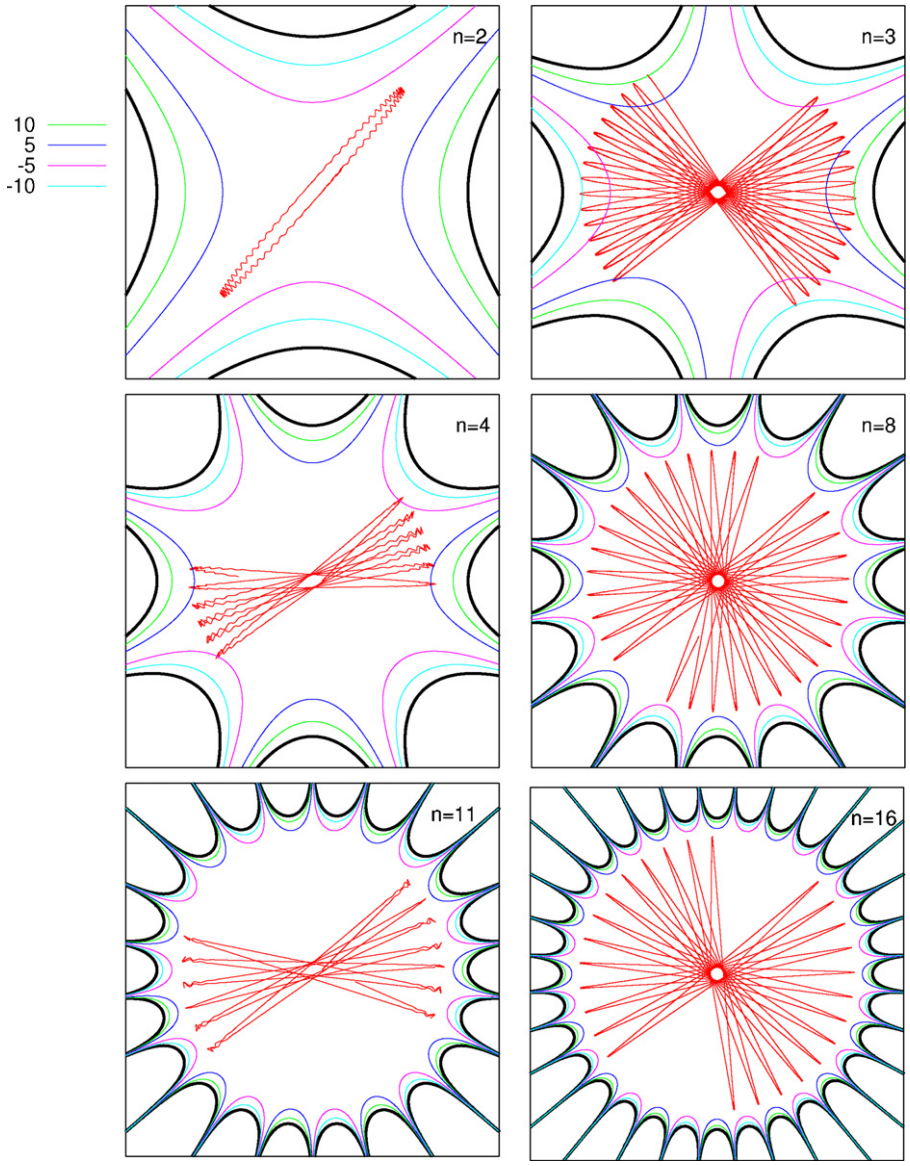

Fig. 3. Visualization of the electric potentials described in Eq. (2) for a fixed time with $\sin(\omega t) = 1$ and several multipolarities n. Voltages of ± 15 V have been applied alternatingly to the hyperbolic electrodes (black lines) and the resulting equipotential lines are shown color-coded. It is clearly seen that the field-free region is increasing for higher n. With these fields varying in a sinusoidal manner $\sin(\omega t)$, some typical ion trajectories are included in each figure. The standard conditions given in Table 1 were used. For better visibility of the ion micromotion, the wiggling motion with frequency f when the ions come close to the electrodes, the RF frequency has been reduced to $f = \omega/2\pi = 5$ MHz in all left-hand sketches.

cylindrical coordinates, and obtaining a new charge distribution using $\rho_{i+1}(r) \sim \exp(-(\Phi_i(r) + \Phi_t(r))/kT)$ where $\Phi_t(r)$ designates the effective trap potential (see e.g., [17]). After a few iterations, the self-consistent charge distribution $\rho(r)$ is found. The static electric field $\vec{E}(r)$ produced by the obtained charge distribution can then be included into the simulations, as shown in Fig. 2, to obtain the ion temperature. As the obtained ion temperature is needed as input for the determination of $\rho(r)$ in the formula above, also a few iterations have to be done for that, starting with a guessed ion temperature.

4. Some test results

In the following, some test runs with the RF and buffer gas subroutines are presented. This serves not only to check their proper operation, but also gives additional insight into the processes occurring in multipole ion traps.

4.1. RF multipole field only

First of all, the RF field of an infinitely long multipole as given by Eq. (3) has been applied and it has been checked that the simulated ion is indeed confined in the radial direction. Ion trajectories as those shown in Fig. 3 were obtained. In general, the ion moves undisturbed in the field-free middle of the trap, and it is only when it comes close to the electrodes that the ion is forced by the RF into a wiggling micromotion with frequency f (clearly visible on the left-hand side of Fig. 3) and is finally reflected away from the electrodes. This motion results in a transversal kinetic ion energy distribution as shown in Fig. 4 for several ideal multipole fields of multipolarity n. The simulations were obtained with the standard conditions (see Table 1) without buffer gas, and the ion was started with an energy E_0 in the middle of the trap towards one of the electrodes. All distributions have a peak at E_0 and this shows indeed that the energy of the ion is recovered when back to the

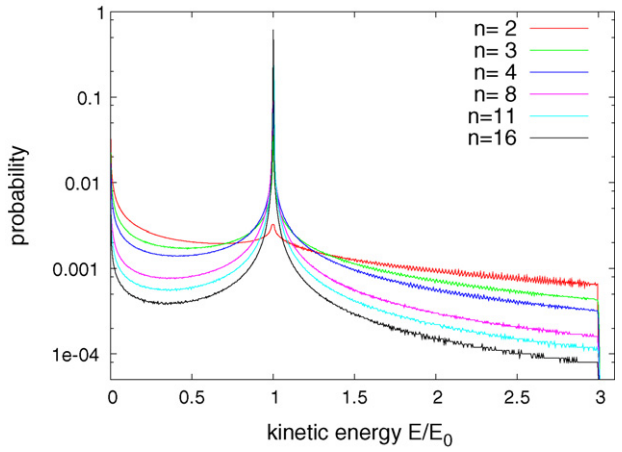

Fig. 4. Kinetic ion energy distribution for the collisionless case. The ion starts with kinetic energy E_0 in the middle of a linear multipole field of multipolarity n. The distributions (600 energy bins) are normalized to the total probability of one. $n = 11$ and $n = 2$ correspond to the 22-pole and the linear quadrupole trap, respectively.

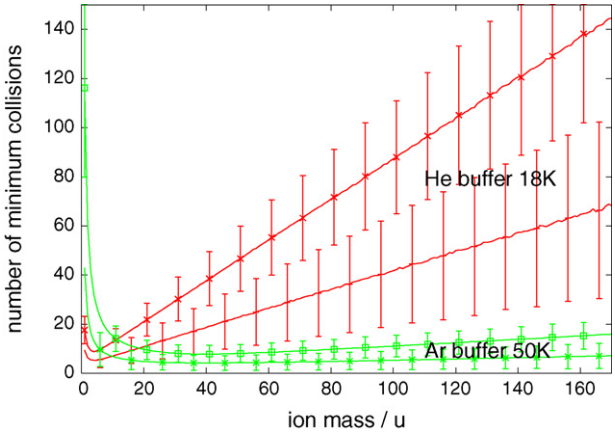

Fig. 5. Number of minimum buffer gas collisions required to cool an ion ensemble with temperature $T_i = 10{,}000$ or 300 K (upper and lower traces, respectively) to the buffer gas temperature T. Two sets of examples are shown, one for a buffer gas with $m_b = 4$ and $T = 18$ K (Helium), and one for buffer gas with $m_b = 40$ and $T = 50$ K (Argon). A minimum of necessary cooling collisions is reached for $m_i = m_b$. The standard deviations are shown only for every tenth point.

middle of the trap, and it is only during the reflection process (see the wiggling motions in Fig. 3) that the ion energy smears out between 0 and a maximum of $3E_0$. A thorough discussion of this behaviour can be found in [17]. Higher order multipole traps, as for example the 22-pole one, possess a wide field-free region. Therefore, the ion moves mostly undisturbed with only short 'hard-wall' reflections, leading to a well-pronounced peak at E_0 seen in Fig. 4.

The fact that the energy E_0 is recovered when the ion is back to the middle of the trap and that even $\langle E \rangle = E_0$ for the whole distribution shows that the RF field itself is not heating the ion in the adiabatic case. It is just in combination with buffer gas collisions (see below) that the ion can gain energy after a reflection from the RF rods.

4.2. Buffer gas only

For testing the buffer gas routine, the RF field has been switched off and an ion with arbitrary initial energy was allowed to collide with buffer gas of temperature T. It has been verified that the ion velocity distribution attained after several hundred collisions indeed corresponds to a Maxwell distribution of temperature T (see the 'no RF' curve in Fig. 6).

Within the given simple collision model also one often-asked question can be readily answered: 'How many collisions does one need to cool an ion with initial temperature T_i to the buffer gas temperature T?' The answer for some selected cases can be found in Fig. 5, where the minimum number of necessary cooling collisions is shown as a function of the ion mass. In these simulations, an ensemble of ions with random velocities corresponding to a temperature $T_i > T$ is relaxed in buffer gas of temperature T, until the ion velocities fall below the mean velocity $\bar{v} = \sqrt{8kT/\pi m_i}$ at temperature T, and the necessary collisions are recorded. As shown in the figure, a minimum of necessary collisions is obtained for the case of equal ion and buffer gas mass. This is for example the case in our experiments where H_2D^+ ions are relaxed in He buffer gas [5,6]. With a buffer gas temperature of $T = 18$ K, about (5 ± 3) collisions are necessary if the ions start with a temperature $T_i = 300$ K, and (9 ± 4) collisions if the initial ion temperature is $T_i = 10{,}000$ K, see Fig. 5. As the internal degrees of freedom of the ion are not taken into account in the model, the given numbers have to be taken as lower limits.

4.3. RF multipole field with buffer gas collisions

Combining the influence of the RF field and the buffer gas collisions, the velocity distribution of an ion in a linear multipole is shown in Fig. 6 applying the standard conditions (Table 1) but for different multipolarities n. Similar simulations have been carried out by Gerlich [17] for the collision of atomic ions with H_2 buffer gas in linear multipoles ($n = 2$, 4, 8) and a ring-electrode trap. It is astonishing that although the RF field and the buffer gas separately do not lead to any heating effects (see preceeding subsections), their combined action does. This 'RF heating effect' is especially pronounced for low multipolarities n due to their lack of a field-free region, as has been recognized in the first days of the Paul trap [31]. For example, in a linear quadrupole ($n = 2$), the ions are about 60 K hotter than the buffer gas (under the specified conditions), while the difference is only 2 K for the 22-pole trap ($n = 11$). This seemingly contradictory heating behaviour is caused by the buffer gas particles dephasing the ion micromotion in the regions of high RF fields near the rods. Depending on of the mass

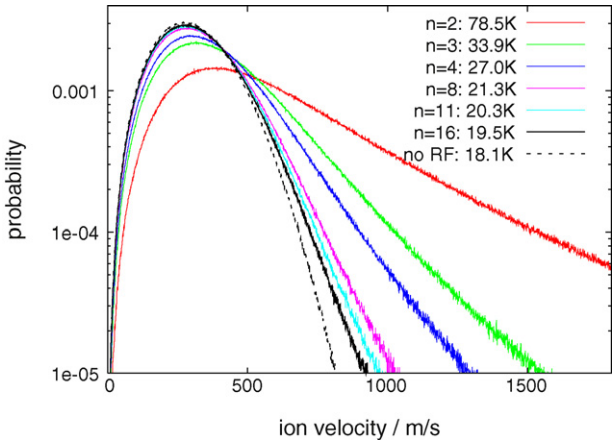

Fig. 6. Velocity distribution (bin width 1 m/s) obtained after 10^7 buffer gas collisions for an ion with mass 4 (and standard conditions, see Table 1) stored in different linear multipole fields. With increasing multipolarity n, the distribution is approaching a Boltzmann distribution with temperature $T = 18$ K, the temperature of the buffer gas. For a 22-pole trap ($n = 11$), the ion temperature is 2 K higher than the buffer temperature.

ratio of the colliding partners this dephasing and thus the heating can be more or less pronounced. In the limiting case of buffer gas particles much heavier than the ion, $m_i < m_b$, this heating effect can be severe (see following section), as the ion can bounce back from the heavier buffer gas atoms as from a hard wall, leading to a 180° phase shift in the oscillatory motion.

5. Ion temperature in a 22-pole trap

In this section we focus on a perfect and infinitely long multipole trap, predominantly a 22-pole trap ($n = 11$), and investigate the dependence of ion temperature on several parameters. As seen in the preceeding section, under the chosen standard conditions, the ions relax to a temperature of 20.3 K in a 22-pole trap. We are interested in the variation of this temperature on changing parameters like the RF amplitude and frequency, the buffer gas mass and collision rate, as well as space charge effects when storing an excessive number of ions. The results are summarized in Fig. 7(a–c).

5.1. Dependence on RF parameters and collision rate

The RF parameters and the collision rate have a negligible impact on the ion temperature as long as they stay within reasonable limits. Changing the collision frequency of the buffer gas between about 1000 s^{-1} and 10^7 s^{-1} does not change remarkably the ion temperature, see Fig. 7(a). For high collision frequencies exceeding the RF frequency, on the other hand, the ions approach the buffer temperature T, being apparently trapped by the buffer gas in the field-free middle of the trap, the initial position of the ions in the simulation. This effect is especially pronounced for the lower multipoles ($n = 2$, 3, 4) in which the ions relax to higher temperatures at low collision frequencies.

Similarly, the RF frequency has no influence on the ion temperature, as long as it is high enough to provide adiabatic conditions (not shown in Fig. 7). Going from 30 MHz to lower frequencies the simulated ion temperature stays at 20 K in a 22-pole trap for the standard conditions. Just below a threshold frequency at about 2 MHz the trajectories become unstable and the ions are eventually lost due to nonadiabatic motion, so that no temperature can be assigned. This behaviour can be calculated analytically by considering the adiabaticity parameter $\eta(\vec{x})$ (for a definition and further relations see [17]), and determining the threshold RF frequency below which the ions moving in an effective trap potential probe trap regions with $\eta \geq 0.3$ and thereby gain energy by nonadiabatic heating. Using a constant ion energy $E = 3/2kT$ ($T = 20$ K), the threshold RF frequency is calculated to be 1.74 MHz. The good agreement with the

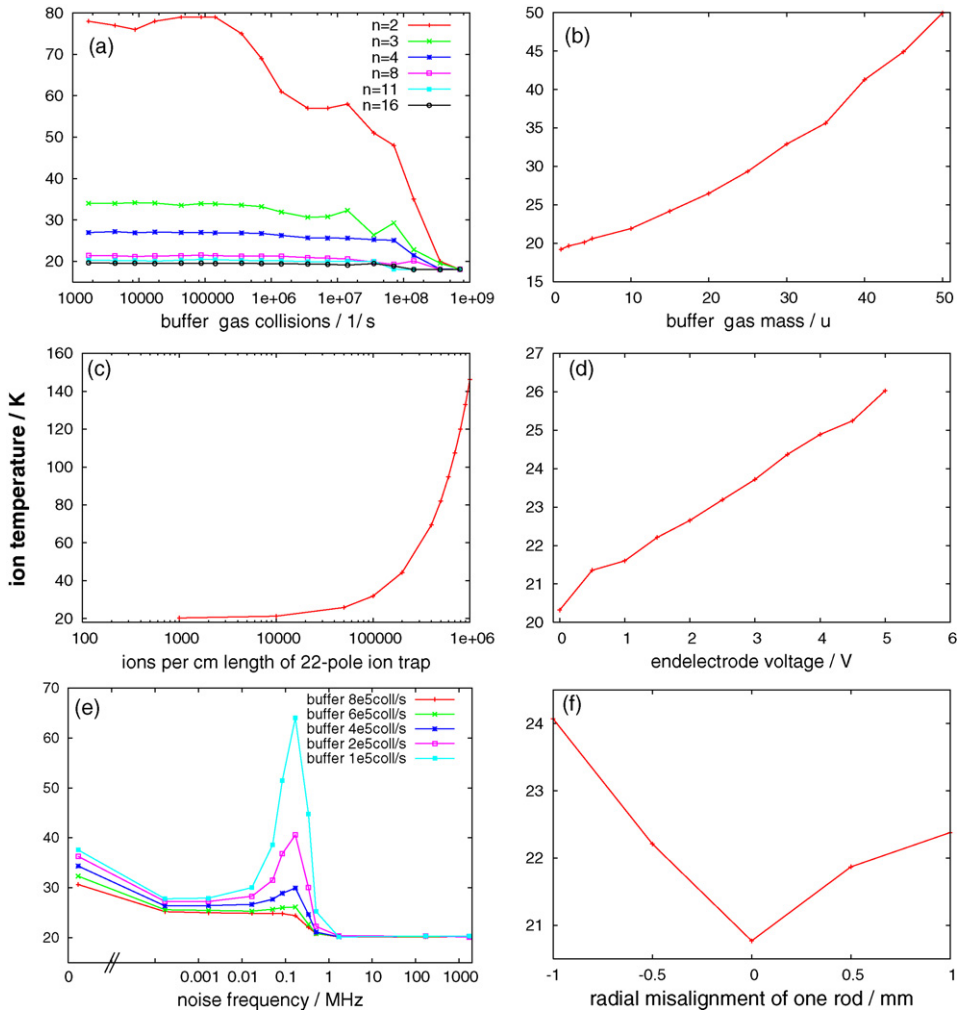

Fig. 7. Dependence of kinetic ion temperature on different parameters and imperfections. The temperatures on the ordinate have been determined by applying Eq. (1) to velocity distributions as those shown in Fig. 6. If not indicated otherwise, the standard conditions given in Table 1 were applied. Shown is the dependence on (a) buffer gas density with multipolatity n as a parameter, (b) dependence on buffer gas mass, (c) dependence on linear density of stored ions, (d) dependence on endelectrode voltage, (e) dependence on RF noise with buffer gas density as a parameter, and (f) dependence on radial misalignment of one rod. For further information, see text.

simulated value serves as a check of the numerical procedure. In fact, the simulated threshold value of 2 MHz is even higher than the calculated value because the Maxwell–Boltzmann distribution allows the ions to have energies more than $3/2kT$.

As explained in Fig. 4 and Section 4.1 the RF field itself does not heat the ions. Accordingly, increasing the RF amplitude, maybe contrary to common intuition, does not lead to any further heating effects in an ideal ion trap. This comes into play only in real ion traps by imperfections of the trap or by direct heating of the trap by the Ohmic losses of the RF power. Increasing the RF amplitude only makes the effective potential steeper, confining the ions to a smaller region. Simulations with RF amplitudes between 15 V and 5000 V show no change in the ion temperature around 20 K. A calculation similar to that given above reveals that for these two parameters the ions are confined to a radial extent of about 0.76 r_0 and 0.43 r_0, respectively. The field-free region is thus shrinked, but this does not have a dramatic effect on the temperature yet.

5.2. Dependence on ion-to-neutral mass ratio

The dependence of the ion temperature on the buffer gas mass is presented in Fig. 7(b), in which it is observed that with increasing mass of the neutral collision partner the ion temperature increases considerably. For example, under the standard conditions, collisions of mass 4 ions with mass 4 neutrals yield a simulated temperature of 20.3 K, while this temperature raises to about 41 K for collisions with mass 40 neutrals. As mentioned before, the heating effect in the case of a heavy neutral can be imagined as originating from ions bouncing back from fixed scattering centers, and when these collisions happen to occur in the RF field, the ion micromotion is strongly disturbed and the ion thus heated. Such kind of heating effect can even lead to the loss of the stored ions, as has been observed for Paul traps [30]. This heating effect is also most probably responsible for the high Doppler temperature of (170 ± 20) K observed by Mikosch et al. [4] for H_3^+ ions embedded in a 55 K gas mixture of Ar and He. The simulations show that an ion temperature of 134 K is obtained for a pure Ar environment. Applying 2 V to the 22-pole endelectrodes (for the additional heating effect of the electrostatic field of the endelectrodes see Section 6), a temperature of 173 K is computed. If the collisions are dominated by 55 K helium buffer gas, the corresponding simulated temperatures are 62 K (no endelectrodes) and 68 K (2 V endelectrodes), respectively.

On the other hand, a very favourable case is given in the cooling of heavy biomolecules with much lighter He atoms in multipole traps [23]. For example, cooling mass 200 protonated biomolecules with 6 K Helium gas in a 22-pole trap, a negligible temperature increase to only 6.7 K is calculated. With such a favourable ion-to-neutral mass ratio, it is stressed that even a simpler octopole trap ($n = 4$) could be used in future experimental setups, in which case the simulations predict a kinetic temperature of 7.7 K, thus an increase of only 1.7 K compared to the helium temperature.

5.3. Dependence on number of stored ions

Usually the number of ions stored in a typical 22-pole trapping experiment, typically about a few thousand, is low enough to avoid space charge effects. If higher numbers of ions are stored, the mutual Coulomb repulsion will push the ions towards the RF electrodes and cause heating. This can be simulated by the numerical procedure described in Section 3.4. The results are depicted in Fig. 7(c) in which the linear ion density of an infinite long 22-pole trap is given on the abscissa. The simulation shows that linear ion densities in the range of some 1000 per cm length are tolerable to maintain cryogenic temperatures, but if the ion number exceeds about 10^5 per cm, the heating becomes severe, and the simulated temperature for a density of 10^6 per cm approaches about 150 K. Heavy loading of a 22-pole trap is only necessary if it is used as an ion source for a storage ring, as is the case at the TSR storage ring in Heidelberg [21]. Although that 22-pole trap is operated at cryogenic temperatures near 10 K, the $\sim 10^6$ stored H_3^+ ions will be heated beyond 160 K by the space charge and the unfavourable 3:4 mass ratio to the Helium buffer gas. This temperature is still favourable compared to an impact ionization source, taking into account the wide rotational level spacing of the stored H_3^+ ions.

6. Impact of endelectrodes

The two endelectrodes of a 22-pole trap (see Fig. 1) confine the stored ions in the longitudinal direction. The electrostatic field of these electrodes has been calculated as explained in Section 3.2 (using a mesh size of 10 μm) and superimposed on the RF field for the simulations in this section. The electrostatic field of the endelectrodes has components in longitudinal as well as radial direction, the latter component leading to a heating effect by pushing the ions into the RF field. Furthermore, the longitudinal and and radial motion of the ions, which were fully independent in the simulations shown until now (except for buffer gas collisions), are coupled by the endelectrode field.

Fig. 7(d) illustrates how the ion temperature is increased by increasing the voltage applied to the endelectrodes. For a typical endelectrode voltage of 1 V (relative to the trap float potential) and for the chosen standard conditions, one obtains a temperature increase of about 1.5 K. This is surely a small change, but the example for $H_3^+ + Ar$ in the preceeding section has shown that the endelectrodes can also have a more dramatic effect for an endelectrode voltage of only 2 V. That this heating effect is caused by the ions being pushed towards the RF electrodes can be seen in Fig. 8, where the transversal ion distribution is shown. For zero voltage applied to the endelectrodes, the ions exhibit a homogeneous transversal distribution, extending about $0.76\,r_0 \approx 4$ mm in the radial direction. By increasing the endelectrode voltage, it can be observed that the ions are more and more likely to be found closer to the RF rods. This behaviour has already been observed experimentally by Trippel et al. [22] in the photodetachment of cold OH^- ions in a 22-pole ion trap. By performing transversal laser scans through the trap the authors showed a higher density of OH^- ions toward the RF electrodes. Similarly, Okada et al. [18] simulated the endelectrode voltage dependence of the crystal structure of laser cooled Ca^+ ions in an octopole trap (see their Fig. 13), and demonstrated in an experiment the breakdown of the crystal behaviour for excessive endelectrode voltages due to the discussed heating effects.

7. Trap imperfections

Some selected imperfections of the 22-pole trap have been simulated in this work and are shown in Fig. 7(e and f). Similar simulations have been performed by Gerlich [17] for an octopole ion guide, taking into account rod misalignment and the charging of one rod (caused for example by an insulating layer).

In the simulation of Fig. 7(e) a small sinusoidal noise signal is overlayed onto the trapping RF voltage (17 MHz, 15 V). The amplitude of the RF noise has been set to 1/100 of the trapping RF voltage (i.e., 0.15 V) and its frequency is shown on the abscissa. Also the case of an electrostatic distortion with a 0.15 V DC difference voltage on the 22 rods has been calculated, found at zero frequency on the abscissa, and indicates a heating to about 37 K for a collision frequency of $10^5\ s^{-1}$. This heating is caused by the attraction of the ion into the RF field around the negatively charged rods. While no heating is calculated for higher noise frequencies, the resonant heating found near 170 kHz for the given trap operating conditions

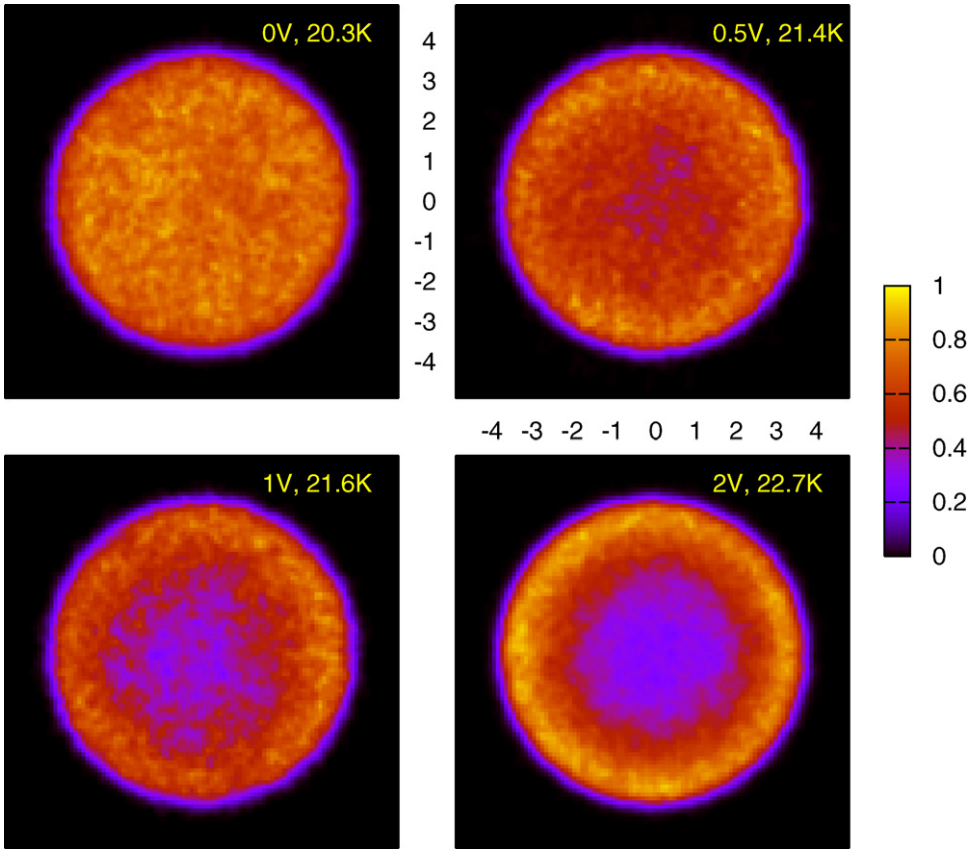

Fig. 8. Color-coded transversal probability distributions of ion with mass 4 in a 22-pole ion trap for different endelectrodes voltages. The view is along the longitudinal axis and the transversal ion positions were recorded without respect of their longitudinal positions. The applied endelectrode voltages and the resulting ion temperatures (compare Fig. 7(d)) are indicated in the figures. The cylindrically symmetric ion cloud has a radius of about 4 mm in all cases. With increasing endelectrode voltage, the ions are pushed closer to the RF rods.

is remarkable. This resonant heating leads to an ion temperature of about 64 K at the standard buffer gas collision frequency, but is strongly dampened for higher buffer gas densities. The frequency of the resonance is related to the secular motion of the ions and therefore to the mean velocity of the ion in the trap. Further simulations indeed show that the resonant frequency depends on the velocity $\bar{v} \sim \sqrt{T/m}$ and thus on the ion temperature T and ion mass m, as well as on the trap dimensions. For these reasons, care has to be taken to avoid lower noise frequency components in multipole ion traps. This is usually accomplished by resonant circuits which admit only the desired RF frequency to the trap rods.

A further possible source of distortion is the misalignment of the trapping rods. In Fig. 7(f) the radial misalignment of a single 22-pole rod has been simulated. As it is no longer possible to express the electric field resulting from the misalignment by the analytical expression (3), the electric potential has been calculated numerically as described in Section 3.2. A cell length of 10 μm has been used in the calculation. Due to this finite size, the temperature obtained for an ideal 22-pole is about 0.4 K higher than for the results using the analytical formula. Nevertheless, the results show that the 22-pole is quite insensitive to rod misalignments. For example, a large radial rod misalignment of 0.5 mm leads to a temperature increase below 1.5 K.

8. Conclusions and outlook

This work was triggered by discrepancies between measured Doppler temperatures of H_2D^+ ions and the nominal temperature of the 22-pole trap they were stored in [5,6]. The simulations clearly show that, assuming a perfect trap, a maximum of about ∼4 K increase above the nominal 18 K (improved to 13 K in the meantime) can be explained by the combined influence of the RF field, the buffer gas, and applying a static voltage of 1 V to the endelectrodes. Space charge effects can be neglected in our case. All other ion heating effects must be due to trap imperfections, ion chemistry, or simply parts of the trap which deviate from the nominal temperature. Concerning the latter argument, it is mentioned that trap temperatures are usually measured on the trap housing, though a large part of the surface seen by the ions and neutrals is given by the trap rods, which could be heated by Ohmic losses in the case of bad thermal anchoring.

In the simulations, it is recalled to pay attention to the ion-to-neutral mass ratio, a fact known since the first days of ion trapping [31]. While for light ions colliding with He buffer gas the use of high-order multipole traps is mandatory for reaching cryogenic temperatures and even severe heating can occur for an unfavourable ratio, for the cryogenic storage of a heavy ion a lower order multipole trap will be sufficient. Also, high endelectrode voltages should be avoided.

The simulations presented here have been mostly applied to the 22-pole trap, but are readily extended to other trap geometries for which the RF field can be given numerically or even analytically. Probably only the space charge calculation become more elaborate as the cylindrical structure of the 22-pole trap allowed a simple treatment. Future simulations will explore in situ mass-selection capabilities, a feature not realized yet in existing multipole traps. Possible directions are the usage of the ring electrodes in 22-pole traps or a multipolar Paul-type trap.

Acknowledgements

This work has been financially supported by the Deutsche Forschungsgemeinschaft (DFG) via SFB494 and the European QUASAAR network. The authors thank Edouard Hugo and Serjoscha Wahed for fruitful discussions and Bernhard Roth and Roland Wester for reading the manuscript prior to publication.

Appendix A. Summary of Langevin theory

Although the Langevin collision theory is very important for many applications, in the literature often substantial errors can be found in the reproductions, much of the confusion probably stemming from using cgi units. Therefore, it is recapitulated here briefly with the correct SI units. The Langevin theory describes the interaction of an ion with charge q with a neutral collision partner with polarizability α. The interaction potential is given by

$$V(r) = -\frac{\alpha}{8\pi\epsilon_0}\frac{q^2}{r^4} \tag{A.1}$$

By considering the effective potential with impact parameter b

$$V_{\text{eff}} = V(r) + E_{\text{kin}}\frac{b^2}{r^2} \tag{A.2}$$

one can derive a maximum impact parameter

$$b_t = \sqrt[4]{\frac{\alpha q^2}{\pi\epsilon_0\mu v^2}} \tag{A.3}$$

below which a collision happens. The parameters μ and v are the reduced mass and the relative velocity, respectively. The cross section $\sigma = \pi b_t^2$ is then

$$\sigma = \frac{q}{v}\sqrt{\frac{\pi\alpha}{\epsilon_0\mu}} \tag{A.4}$$

The rate coefficient $k_L = \sigma v$ is then finally obtained

$$k_L = q\sqrt{\frac{\pi\alpha}{\epsilon_0\mu}} \tag{A.5}$$

which in practical units (α in Å^3, μ in u, k_L in cm^3 s^{-1}) can be written

$$k_L = 2.342\sqrt{\frac{\alpha}{\mu}}10^{-9}\ \text{cm}^3\ \text{s}^{-1} \tag{A.6}$$

References

[1] T.W. Hänsch, A.L. Schawlow, Opt. Commun. 13 (1975) 68.
[2] W. Neuhauser, M. Hohenstatt, P. Toschek, H. Dehmelt, Phys. Rev. Lett. 41 (1978) 233.
[3] D.J. Larson, J.C. Bergquist, J.J. Bollinger, W.M. Itano, D.J. Wineland, Phys. Rev. Lett. 57 (1986) 70.
[4] J. Mikosch, H. Kreckel, R. Wester, R. Plašil, J. Glosík, D. Gerlich, D. Schwalm, A. Wolf, J. Chem. Phys. 121 (2004) 11030.
[5] O. Asvany, E. Hugo, F. Müller, F. Kühnemann, S. Schiller, J. Tennyson, S. Schlemmer, J. Chem. Phys. 127 (2007) 154317.
[6] O. Asvany, O. Ricken, H.S.P. Müller, M.C. Wiedner, T. Giesen, S. Schlemmer, Phys. Rev. Lett. 100 (2008) 233004.
[7] D. Gerlich, E. Herbst, E. Roueff, Planetary Space Sci. 50 (2002) 1275.
[8] S. Schlemmer, O. Asvany, E. Hugo, D. Gerlich, in: D. Lis, G. Blake, E. Herbst (Eds.), IAU Symposium 231, 2006.
[9] R. Otto, J. Mikosch, S. Trippel, M. Weidemüller, R. Wester, Phys. Rev. Lett. 101 (2008) 063201.
[10] E. Fischer, Zeitschrift für Physik 156 (1959) 1.
[11] W. Paul, Electromagnetic traps for charged and neutral particles, Nobel Lecture, 1989, available on www.nobel.se.
[12] R.F. Wuerker, H. Shelton, R.V. Langmuir, J. Appl. Phys. 30 (1959) 342.
[13] P.H. Dawson, N.R. Whetten, J. Vac. Sci. Technol. 5 (1967) 1.
[14] F.A. Londry, R.L. Alfred, R.E. March, J. Am. Soc. Mass Sprectrom. 4 (1993) 687.
[15] J. Parks, A. Szöke, J. Chem. Phys. 103 (1995) 1422.
[16] C.B. Zhang, D. Offenberg, B. Roth, M.A. Wilson, S. Schiller, Phys. Rev. A 76 (2007) 012719.
[17] D. Gerlich, in: C.-Y. Ng, M. Baer (Eds.), Adv. Chem. Phys.: State-Selected and State-to-State Ion-Molecule Reaction Dynamics, vol. LXXXII, Wiley, New York, 1992, p. 1.
[18] K. Okada, K. Yasuda, T. Takayanagi, M. Wada, H.A. Schuessler, S. Ohtani, Phys. Rev. A 75 (2007) 033409.
[19] D. Gerlich, Phys. Scr. T59 (1995) 256.
[20] O. Asvany, P. Kumar, B. Redlich, I. Hegemann, S. Schlemmer, D. Marx, Science 309 (2005) 1219.
[21] A. Wolf, H. Kreckel, L. Lammich, et al., Phil. Trans. R. Soc. A 364 (2006) 2981.
[22] S. Trippel, J. Mikosch, R. Berhane, R. Otto, M. Weidemüller, R. Wester, Phys. Rev. Lett. 97 (2006) 193003.
[23] O.V. Boyarkin, S.R. Mercier, A. Kamariotis, T.R. Rizzo, J. Am. Chem. Soc. 128 (2006) 2816.
[24] A. Dzhonson, D. Gerlich, E.J. Bieske, J.P. Maier, J. Mol. Str. 795 (2006) 93.
[25] I. Savić, D. Gerlich, PCCP 7 (2005) 1026.
[26] Y.-S. Wang, C.-H. Tsai, Y.T. Lee, H.-C. Chang, J.C. Jiang, O. Asvany, S. Schlemmer, D. Gerlich, J. Phys. Chem. A 107 (2003) 4217.
[27] R. Feynman, R. Leighton, M. Sands, The Feynman Lectures on Physics, vol. 1, Sec. 9–6, Addison-Wesley, 1963.
[28] SIMION 3D Version 7.0, Idaho National Engineering and Environmental Laboratory.
[29] W.H. Press, S.A. Teukolsky, W.T. Vetterling, B.P. Flannery, Numerical Recipies, Cambridge University Press, 2007.
[30] A. Alili, J. André, F. Vedel, Phys. Scr. T22 (1988) 325.
[31] F.G. Major, H.G. Dehmelt, Phys. Rev. 170 (1968) 91.